NASA TN D-1505

TECHNICAL NOTE

D-1505

THE BENDING-MOMENT DISTRIBUTION OF CAMBERED-SPAN WING SYSTEMS HAVING MINIMUM INDUCED DRAG

By Clarence D. Cone, Jr.

Langley Research Center
Langley Station, Hampton, Va.

NATIONAL AERONAUTICS AND SPACE ADMINISTRATION
WASHINGTON
March 1963

Copy 1

Code 1

CONTENTS

NATIONAL AERONAUTICS AND SPACE ADMINISTRATION

TECHNICAL NOTE D-1505

THE BENDING-MOMENT DISTRIBUTION OF CAMBERED-SPAN WING SYSTEMS HAVING MINIMUM INDUCED DRAG

By Clarence D. Cone, Jr.

SUMMARY

The basic integral equations for determining the bending-moment distributions of optimally loaded cambered-span wing systems are derived and applied to the calculation of the moment distributions for the families of circular-arc and semiellipse camber forms. The effects of the type and amount of camber on the moment distribution are investigated, and it is shown that spanwise camber results in an appreciable increase in the local bending moment near the tips, as compared with that of flat wings furnishing equal lift. The quantitative relation between the magnitude of the bending moment and the induced-drag efficiency of cambered-span wings is developed.

A simple analysis is carried out to establish the wing structural requirements dictated by the bending-moment distribution, and a procedure is outlined for determining the optimum chord distribution of the wing for obtaining minimum profile drag.

INTRODUCTION

The theoretical possibilities of increasing the aerodynamic efficiency of lifting systems having limited projected span lengths by use of cambered-span airfoils are discussed in detail in reference 1. The design procedures for optimizing the aerodynamic efficiency of cambered wings at cruise conditions are outlined in reference 2. In both of these papers it is explicitly pointed out that the possibility of obtaining useful increases in flight efficiency with cambered-span wings, as compared with flat wings of equal projected span, depends entirely upon the ability to construct cambered wings with sufficiently low profile-drag coefficients and structural weights. Hence, in design analyses intended to evaluate the relative efficiency of cambered wings for specific applications, it is necessary to consider the effects of the aerodynamic force and moment distributions on the structural characteristics of the wing and also the associated effects of the structural characteristics on the wing profile drag.

Of special importance in this respect is a knowledge of the bending-moment distribution associated with the optimum aerodynamic loading of cambered-span

wings. The curvature of such wings produces lateral components of the local aerodynamic forces, in addition to the lift or vertical components, and these additional forces can increase the magnitude of the bending-moment distribution along the wing, as compared with the distribution along a flat wing of equal projected span, for the same total lift force. Since the minimum spar depth of a wing is in many cases governed by the bending-moment distribution, if the use of excessively heavy spars is to be avoided the minimum allowable profile thickness will be governed by the bending-moment distribution. Thus, if the wing bending moments are excessively large, the minimum attainable profile thickness may be of such a magnitude that the wing profile drag becomes prohibitively large.

In order that such aerodynamic-structural relationships may be included in the overall design and efficiency evaluation of cambered-span wings, this paper develops the basic relations necessary for determining the bending-moment distribution of any optimally loaded cambered wing form, and formulates some general relations for use in comparing the effects of various forms and amounts of spanwise camber on the bending moments. In particular, nondimensionalized bending-moment distributions are determined for the families of circular-arc and semi-ellipse camber lines. The relation between the magnitude of the bending moment and the induced-drag efficiency is derived, and a procedure is presented for determining the optimum wing chord distribution for minimum profile drag when the section thickness is known.

The relations developed are for the case of wings having simple camber forms. (See ref. 1.) The results may be applied, however, to the analysis of more complex forms, such as wings having closed-arc or branched tips, by summing the moment contributions of the various elements of the total wing system.

Although the considerations herein are discussed primarily in relation to airfoils, it should be noted that the general features of the analysis also apply directly to the case of water-based lifting systems such as nonplanar hydrofoil systems having centrally located support struts.

SYMBOLS

B constant, $\int_{-1}^{1} \frac{\Gamma}{\Gamma_o}(\gamma)d\gamma$

b span of flat-span reference wing

b' projected span of cambered-span wing

c wing chord length

c_d section drag coefficient

c_l section lift coefficient

C_1	value of k for $\psi = 1.0$
C_2	moment-of-inertia constant
D_o'	profile-drag force intensity
d	spanwise-camber depth (fig. 3)
E	modulus of elasticity
F'	aerodynamic-force loading intensity (fig. 2)
f	camber-line function
f'	derivative of camber-line function
h	maximum-stress distance factor
I	area moment of inertia of wing spar
K	camber function, circular arcs
k	induced-drag efficiency factor
L	total vertical lift
L'	lift loading intensity
M	bending-moment distribution (moment positive in counterclockwise direction; see fig. 2)
M'	nondimensional form of M
N_A	constant, $\frac{\Gamma_o/w_o}{b'/2}$
n	neutral-axis distance factor, $2h/t$
P	bending moment ratio function
q	dynamic pressure, $\frac{1}{2}\rho V^2$
q_Σ	wake induced velocity at wing (vertical for wings having a plane of symmetry)
R	local radius of curvature of neutral axis of spar
r	radius of curvature of circular arc
s	arc-length coordinate (fig. 1)

s_T total arc length of spanwise camber line, eq. (35)

s' variable coordinate of spanwise camber line

t section profile thickness

V flight velocity

W total load carried by wing

w_o downwash velocity far behind wing

Y' side-force loading intensity

y,z Cartesian coordinates of spanwise camber line

Z section modulus, I/h

β camber factor, $\frac{d}{b'/2}$

Γ local circulation distribution

Γ_o circulation of root section

γ nondimensional coordinate, $\frac{y}{b'/2}$

δ nondimensional coordinate, $\frac{z}{b'/2}$

ϵ constant, $2C_2$

θ flexural stress

λ nondimensional coordinate, $\frac{\eta}{b'/2}$

μ thickness ratio, t/c

ξ,η Cartesian coordinates of a variable point on spanwise camber line

ρ mass density

σ nondimensional coordinate, $\frac{\xi}{b'/2}$

τ slope of camber-line tangent, $\tan^{-1}\frac{dz}{dy}$

φ eccentric angle of ellipse

φ' dummy variable of integration (eq. (A5))

ψ span ratio, b/b'

ω maximum-stress ratio, $\frac{M_{max}}{\theta_{max}}$

Subscripts:

c cambered-span wing

D design condition

eff effective

f flat-span wing

max maximum

min minimum

opt optimum

t tip

ξ property at ξ

1 circular-arc camber line

2 semiellipse camber line

THE OPTIMUM LIFT DISTRIBUTION

It is shown in reference 1 that when a cambered-span wing is considered as a bound vortex line (fig. 1) the wing will possess a minimum induced drag for a given vertical lift when the distribution of circulation $\Gamma(s)$ along the line is such that the component of the wake induced velocity normal to the line at every point has the value

$$(q_\Sigma)_{eff} = \frac{w_o}{2} \cos \tau \qquad (1)$$

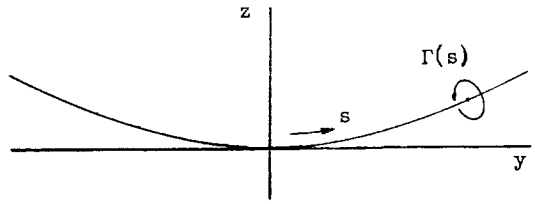

Figure 1.- Coordinate system of a lifting arc.

It is further shown in this reference that the optimum circulation distribution can be obtained by use of conformal transformation techniques or, experimentally, by use of an electrical potential-flow analog. The optimum distribution in the nondimensional form $\frac{\Gamma}{\Gamma_o}(s)$ is a function only of the shape of the span camber line $z(y)$, or $\delta(y)$. The aerodynamic-force intensity $F'(s)$ along the lifting line is then obtained from the Kutta-Joukowski theorem as

$$F'(s) = \rho V \Gamma_o \frac{\Gamma}{\Gamma_o}(s) \tag{2}$$

This distribution of the local aerodynamic force, corresponding to minimum induced drag for a given vertical lift L, determines a corresponding bending-moment distribution along the wing.

In practice, cambered wings are designed to attain minimum total drag at the "design" flight conditions of the particular aircraft mission under consideration (ref. 2), and the lift distribution will be that for minimum induced drag. At conditions other than those of design flight, such as deviations of the local angle of attack or dynamic pressure from the optimum values, the wing force distribution will be somewhat different with a corresponding alteration of the (nondimensional) bending-moment distribution. For moderate variations, however, it is not to be expected that the nondimensional moment distribution will be significantly different from that for the design condition. Consequently, for the purposes of this paper, it is assumed that the nondimensional bending-moment distribution corresponds to the optimum lift distribution in all cases.

THE BENDING-MOMENT DISTRIBUTION AT OPTIMUM LOADING

In this section, the generalized integral equation is derived for the bending-moment distribution along the arc of a curved wing having a camber line of arbitrary form $z(y)$ and supporting a given load W. It is assumed throughout the analysis that the camber line is optimally loaded; that is, the circulation distribution $\Gamma(s)$ is that necessary for minimum induced drag. The dimensional form of the integral is considered first.

The Dimensional Moment Distribution

The aerodynamic-force loading intensity F' acting at the local point s' of the lifting arc of figure 2 can be resolved into the components

$$L' = F' \cos \tau \tag{3}$$

and

$$Y' = F' \sin \tau \tag{4}$$

where τ is the inclination of the tangent to the camber line. By denoting the position of point s' by its corresponding Cartesian coordinates (ξ,η), the differential of bending moment at the fixed point $s(y,z)$ due to the loading at the variable point s' is given by

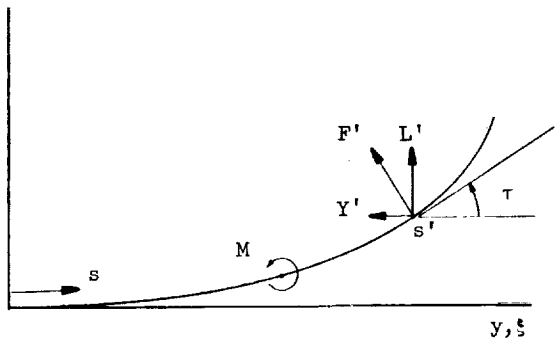

Figure 2.- Local-force intensity components.

$$dM = \left[F'(\xi - y)\cos \tau_\xi + F'(\eta - z)\sin \tau_\xi\right]ds' \tag{5}$$

where the subscript ξ denotes that τ is to be evaluated at the variable point (ξ,η). The total bending moment at the fixed point s due to the total aerodynamic load outboard of the point is then given by

$$M(s) = \int_s^{s_t} \left[F'(s')\ (\xi - y)\cos \tau_\xi + F'(s')\ (\eta - z)\sin \tau_\xi\right]ds' \tag{6}$$

and, since the limit s applies to any point on the semispan, this equation specifies the bending-moment distribution for the wing. It is obvious that, since the lifting elements of the cambered wing are not confined to a horizontal plane, additional bending-moment contributions arise from the side-force components as compared with a flat wing having the same distribution of vertical lift. In the limiting case of a flat-span wing, equation (6) reduces to

$$M(y) = \int_y^{b'/2} F'(\xi)\ (\xi - y)d\xi \tag{7}$$

In equation (6) the aerodynamic-force loading intensity $F'(s')$ is given by

$$F'(s') = \rho V \Gamma(s') \tag{8}$$

where $\Gamma(s')$ is the circulation distribution corresponding to the optimum loading for minimum induced drag. Then, since

$$\left.\begin{aligned} \cos \tau_\xi\ ds' &= d\xi \\ \sin \tau_\xi\ ds' &= d\eta \end{aligned}\right\} \tag{9}$$

the bending moment can be expressed as a function of y in the form

$$M(y) = \rho V \Gamma_o \left[\int_y^{b'/2} \frac{\Gamma}{\Gamma_o} (\xi - y) d\xi + \int_z^d \frac{\Gamma}{\Gamma_o} (\eta - z) d\eta \right] \tag{10}$$

In equation (10) Γ/Γ_o is the optimum nondimensional circulation distribution as determined by either the conformal transformation or electrical analog method of reference 1, and (z,y) and (η,ξ) are related by the camber-line equation

$$\left.\begin{aligned} z &= f(y) \\ \eta &= f(\xi) \end{aligned}\right\} \tag{11}$$

where f denotes the same functional relation. The integral limit d corresponds to the vertical coordinate of the wing tip $z_t = d$. By using the relations of equations (11) and the differential expression

$$d\eta = f'(\xi) d\xi \tag{12}$$

the second integral in equation (10) becomes

$$\int_z^d \frac{\Gamma}{\Gamma_o} (\eta - z) d\eta = \int_y^{b'/2} \frac{\Gamma}{\Gamma_o} \left[\left(f(\xi) - f(y) \right] f'(\xi) d\xi \right. \tag{13}$$

and the bending-moment distribution $M(y)$ is then given by

$$M(y) = \rho V \Gamma_o \int_y^{b'/2} \frac{\Gamma}{\Gamma_o}(\xi) \left\{ (\xi - y) + \left[f(\xi) - f(y) \right] f'(\xi) \right\} d\xi \tag{14}$$

It should perhaps be noted here that $\frac{\Gamma}{\Gamma_o}(\xi)$ is the new function obtained by stating the circulation Γ at corresponding points ξ and s. Since the relation between the arc-length coordinate s and the Cartesian coordinate y of the camber line is obtained from

$$s = \int_0^y \sqrt{1 + \left(\frac{d\eta}{d\xi} \right)^2} \, d\xi \tag{15}$$

the moment distribution $M(s)$ along the camber line follows directly from equation (14).

The total vertical lift force L of a cambered-span wing is given by

$$L = \rho V \Gamma_o \int_{-s_t}^{s_t} \frac{\Gamma}{\Gamma_o}(s) \cos \tau \, ds \tag{16}$$

or by using the nondimensional coordinate $\gamma = \frac{y}{b'/2}$

$$L = \rho V \Gamma_o \frac{b'}{2} \int_{-1}^{1} \frac{\Gamma}{\Gamma_o}(\gamma)d\gamma \tag{17}$$

As shown in reference 1, the integral of equation (17) is a dimensionless constant for any particular camber form for the optimally loaded condition, that is,

$$\int_{-1}^{1} \frac{\Gamma}{\Gamma_o}(\gamma)d\gamma = B \tag{18}$$

Hence, if in flight the wing supports a total load W with an optimum load distribution, then $L = W$ and the circulation Γ_o in the wing plane of symmetry is obtained from the relation

$$\Gamma_o = \frac{W}{\rho V \frac{b'}{2} B} \tag{19}$$

The corresponding wing bending-moment distribution in terms of the wing span and load carried is obtained from equation (14) in the form

$$M(y) = \frac{W}{\frac{b'}{2} B} \int_{y}^{b'/2} \frac{\Gamma}{\Gamma_o}(\xi)\left\{(\xi - y) + \left[f(\xi) - f(y)\right] f'(\xi)\right\} d\xi \tag{20}$$

The moment distribution $M(s)$ along the curved span is obtained by use of equation (15).

The Nondimensional Moment Distribution

Equation (20) of the preceding section can be nondimensionalized by dividing all distances by $b'/2$. With the following definitions

$$\left.\begin{aligned} \delta &= \frac{z}{b'/2} \\ \gamma &= \frac{y}{b'/2} \\ \lambda &= \frac{\eta}{b'/2} \\ \sigma &= \frac{\xi}{b'/2} \end{aligned}\right\} \tag{21}$$

the moment distribution becomes

$$M'(\gamma) = \frac{M(\gamma)}{W\frac{b'}{2}} = B^{-1}\int_{\gamma}^{1}\frac{\Gamma}{\Gamma_o}(\sigma)\left\{(\sigma - \gamma) + \left[f(\sigma) - f(\gamma)\right]f'(\sigma)\right\}d\sigma \qquad (22)$$

For a specific nondimensional camber form given by $\delta = f(\gamma)$, or $\lambda = f(\sigma)$, where f is the characteristic function of the camber form, the right-hand side of equation (22) is a function only of the dimensionless span coordinate γ, since the function M' depends only upon the shape of the camber line when the wing is optimally loaded.

The dimensional bending-moment distribution $M(y)$ (or the corresponding function $M(s)$) of any given size wing is obtained directly from equation (22) by multiplying M' by the load W and semispan length $b'/2$; thus,

$$M(y) = W\frac{b'}{2}M'(\gamma) \qquad (23)$$

where $y = \gamma\frac{b'}{2}$ gives the dimensional coordinate y corresponding to the nondimensional coordinate γ. In effect, the value of M' for a particular value of γ represents the fraction of the "reference" moment $W\frac{b'}{2}$ which acts at that point of the span. In particular, the root bending moment $M(0)$ is given by

$$M(0) = W\frac{b'}{2}M'(0) = W\frac{b'}{2}\cdot \text{Constant} \qquad (24)$$

where the constant depends only upon the camber form f.

THE BENDING-MOMENT DISTRIBUTION FOR FAMILIES OF CAMBERED LIFTING LINES

As an example of the application of the relations derived in the previous section and in order to obtain information for later use, the nondimensional bending-moment distributions for two families of camber lines are now derived.

Circular-Arc Lifting Lines

The equation of the symmetrical circular-arc segment (see fig. 3) is

$$z = r - \left(r^2 - y^2\right)^{1/2} \qquad \left(0 \leqq y \leqq \frac{b'}{2}\right) \qquad (25)$$

Writing equation (25) in nondimensional form by dividing by $b'/2$ gives the following result:

$$\delta = \frac{r}{b'/2} - \left[\left(\frac{r}{b'/2}\right)^2 - \gamma^2\right]^{1/2} \qquad (26)$$

If the particular arcs of the family are denoted by their camber factor β, where $\beta = \frac{d}{b'/2}$ (fig. 3), the camber-line equation of the entire family can be written. Thus, in terms of β, the radius for circular arcs is given by

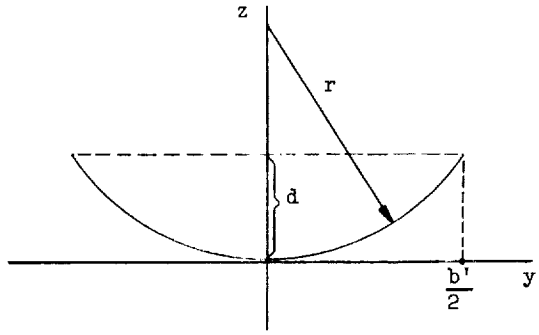

Figure 3.- Geometrical relations for a circular arc.

$$\frac{r}{b'/2} = \frac{1 + \beta^2}{2\beta} = K(\beta) \qquad (27)$$

and equation (26) becomes

$$\delta = f_1(\gamma) = K(\beta) - \left[K^2(\beta) - \gamma^2\right]^{1/2} \qquad (28)$$

In terms of the local variables σ and λ equation (26) is given by

$$\lambda = f_1(\sigma) = K(\beta) - \left[K^2(\beta) - \sigma^2\right]^{1/2} \qquad (29)$$

Differentiation of equation (29) gives the nondimensional form of $f'_1(\sigma)$ as

$$f'_1(\sigma) = \frac{\sigma}{\left(K^2 - \sigma^2\right)^{1/2}} \qquad (30)$$

The substitution of equations (28), (29), and (30) into equation (22) and use of the functions $B(\beta)$ and $\frac{\Gamma}{\Gamma_o}(\sigma,\beta)$ given in figure 4 allow the determination of $M'(\gamma)$ for any desired value of β by carrying out the integration indicated. The values of B and Γ/Γ_o presented in figure 4 were determined by conformal transformation.

The integration of equation (22) for the case of circular arcs has been performed numerically by machine computation, and the results are presented in figure 5. It is obvious that the local bending moments increase appreciably as the camber is increased while a constant projected span length and vertical lift are maintained.

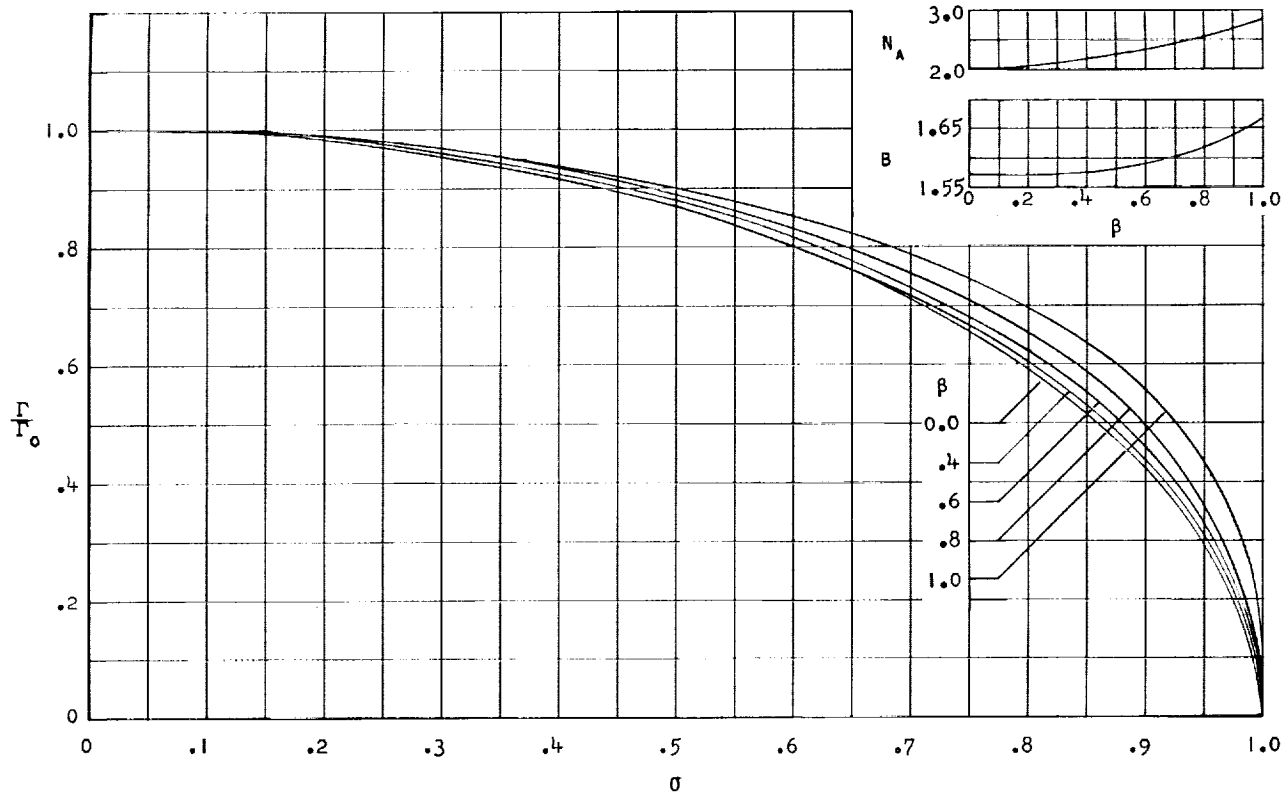

Figure 4.- Variation of the optimum nondimensional circulation distribution and efficiency constants of circular-arc camber lines with degree of camber.

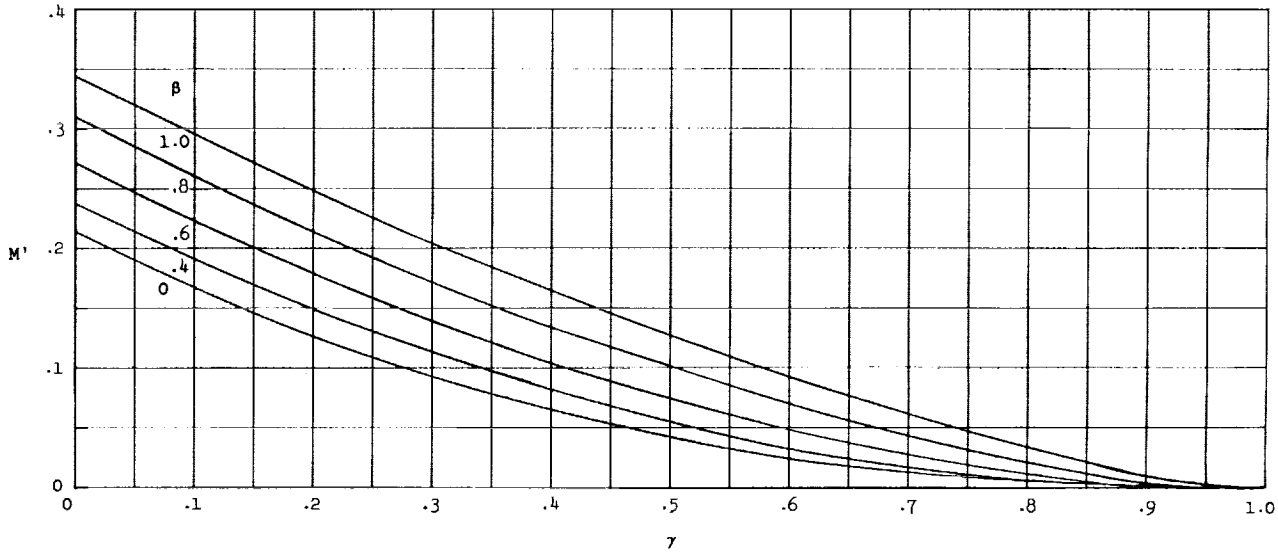

Figure 5.- Bending-moment distributions of circular arcs.

The dimensional moment distribution for a wing with circular-arc camber having any specified semispan length and total lift can be obtained from equation (23) as a function of y, and then determined as a function of the arc-length coordinate s by use of equation (15). For the circular-arc camber line, equation (15) yields

$$s(y) = \frac{b'}{4} \frac{1 + \beta^2}{\beta} \sin^{-1}\left[\frac{4\beta y}{b'(1 + \beta^2)}\right]$$

Semiellipse Lifting Lines

From the geometrical relations of figure 6, the equation of the symmetrical semiellipse camber line is

$$\frac{(z - d)^2}{d^2} + \frac{y^2}{\left(\frac{b'}{2}\right)^2} = 1 \qquad (31)$$

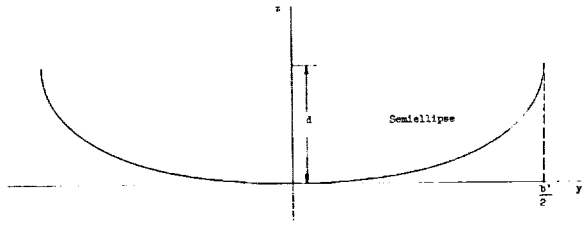

Figure 6.- Geometry of the ellipse.

Employing the camber factor $\beta = \frac{d}{b'/2}$ in equation (31) gives

$$\frac{\left(z - \beta \frac{b'}{2}\right)^2}{\beta^2\left(\frac{b'}{2}\right)^2} + \frac{y^2}{\left(\frac{b'}{2}\right)^2} = 1 \qquad (32)$$

and the nondimensional equation of the semiellipse camber line follows directly as

$$\frac{(\delta - \beta)^2}{\beta^2} + \gamma^2 = 1 \qquad (33)$$

The basic relations for calculating the bending-moment distribution are thus given by

$$\left.\begin{aligned} \delta &= f_2(\gamma) = \beta - \beta\sqrt{1 - \gamma^2} \\ \lambda &= f_2(\sigma) = \beta - \beta\sqrt{1 - \sigma^2} \\ f'_2(\gamma) &= \beta \frac{\sigma}{\sqrt{1 - \sigma^2}} \end{aligned}\right\} \qquad (34)$$

and the functions $B(\beta)$ and $\frac{\Gamma}{\Gamma_o}(\sigma,\beta)$ for the semiellipse form are given in figure 7. These latter functions were determined by use of the analog technique

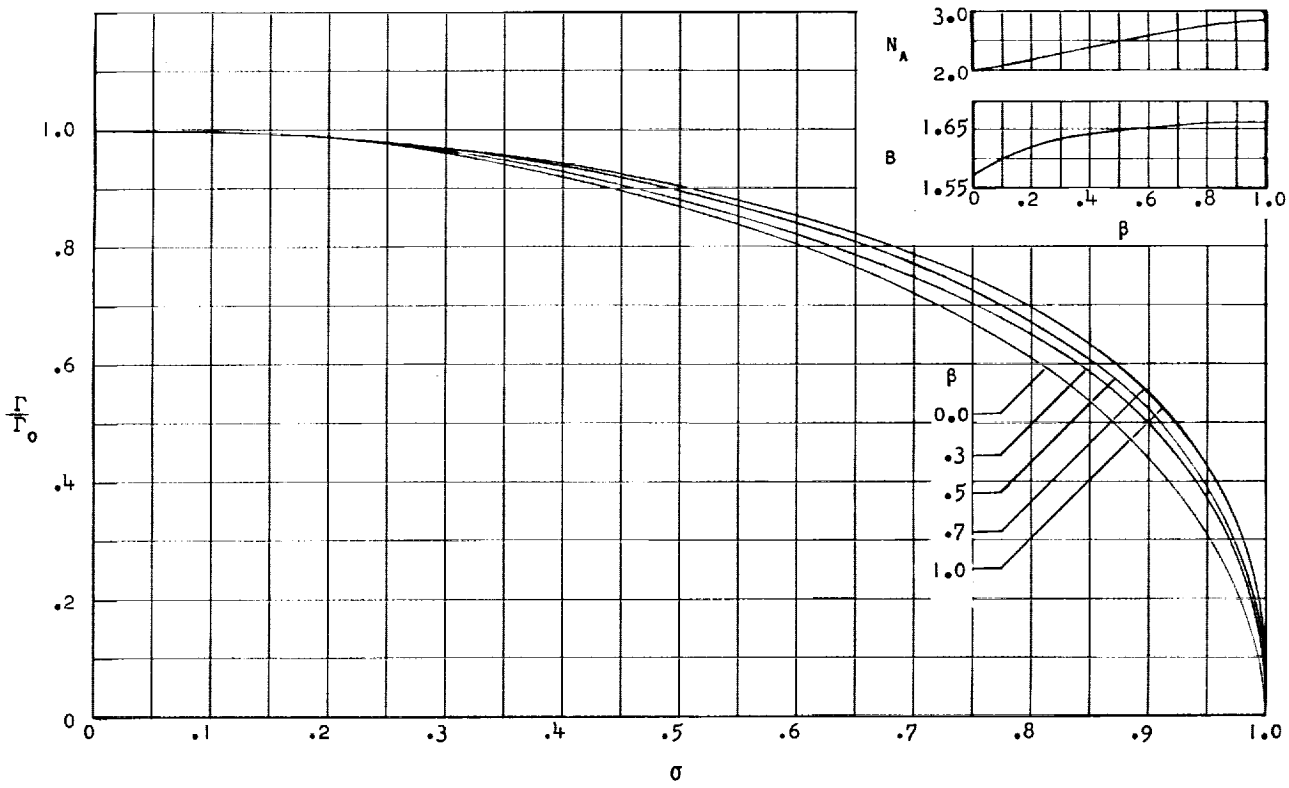

Figure 7.- Variation of the optimum nondimensional circulation distribution and efficiency constants of semiellipse camber lines with degree of camber.

discussed in reference 1. With use of these relations, equation (22) has been integrated to obtain the nondimensional bending-moment function $M'(\gamma)$ for the family $0 \leqq \beta \leqq 1$ of semiellipse camber lines, and the results are presented in figure 8. The moment distributions are very similar to those of figure 5 for circular-arc forms.

The dimensional distribution $M(y)$ is obtained by use of figure 8 and equation (23). The function $M(s)$ can then be determined by use of equation (15). Application of equation (15) leads to an elliptical integral for the case of semiellipse camber forms, and thus s cannot be expressed as a function of y in simple form. The integration of equation (15) for the entire family of semiellipse forms $0 \leqq \beta \leqq 1$ has been carried out by numerical methods (as shown in the appendix), and the results are presented in nondimensional form in figure 9.

EFFECT OF CAMBER ON THE BENDING MOMENT

An optimally loaded camber-span wing of projected semispan $b'/2$ furnishing a vertical lift force L will theoretically have an induced drag $1/k$ times that of an elliptically loaded flat wing of semispan $b/2$ furnishing the same lift, where the efficiency factor k is a function only of the camber factor β

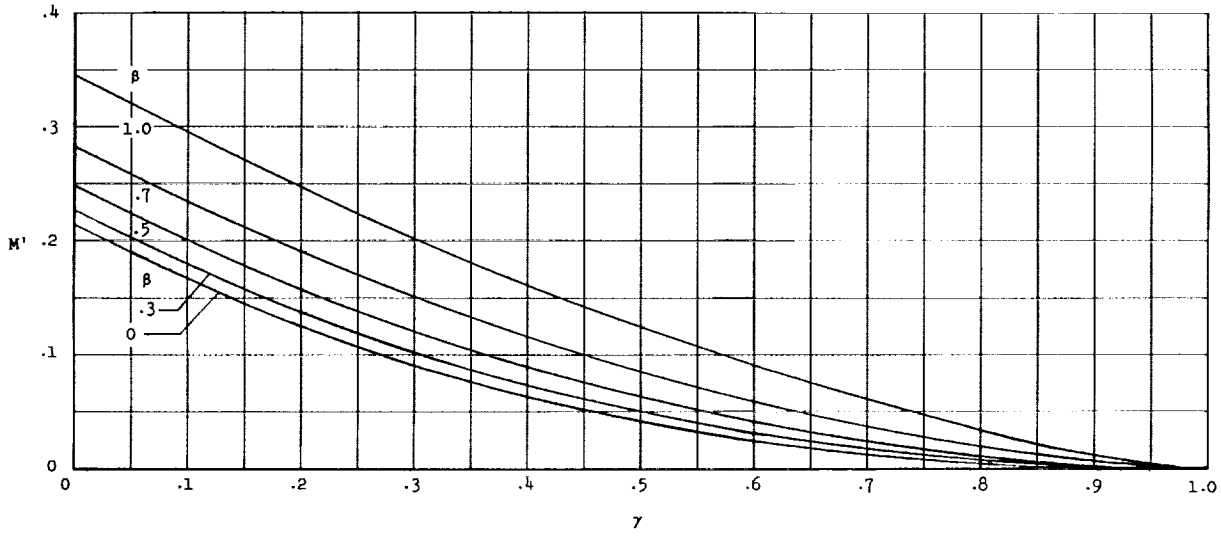

Figure 8.- Bending-moment distributions for semiellipses.

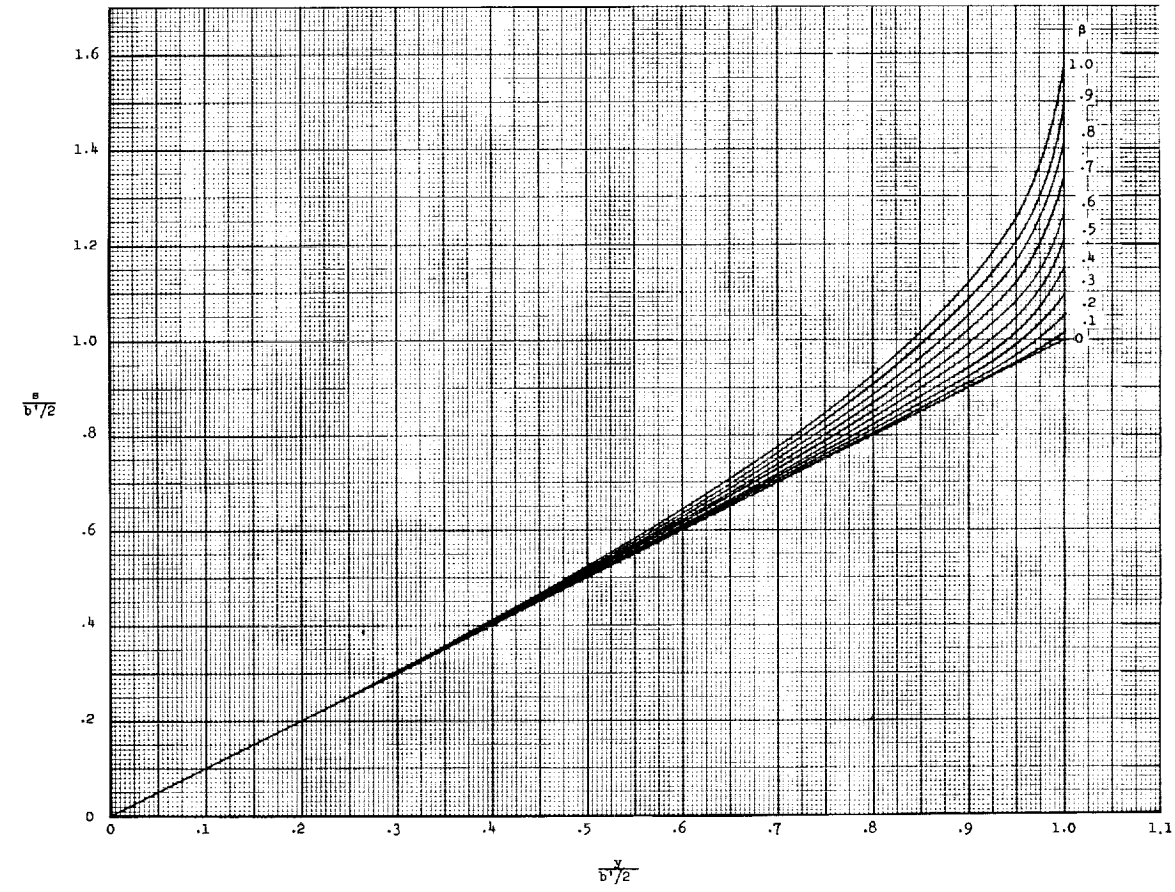

Figure 9.- Relation between arc-length coordinate s and Cartesian coordinate y for semiellipse forms.

and the span ratio $\psi = \frac{b/2}{b'/2}$ for any particular camber form. (See ref. 1.) In the particular case where a cambered wing is compared with a flat wing of equal projected semispan ($\psi = 1$), the value of k is greater than 1.0 so that the induced drag of the cambered wing is less than that of the flat wing. However, the profile drag of the curved wing may be larger than that of the flat wing since the total arc length of the curved span will be greater than the flap span when $\psi = 1$. It is also possible that the structural weight of the curved wing may exceed that of the flat wing because of the longer physical span s_T where

$$s_T = \int_{-s_t}^{s_t} ds = \int_{-b'/2}^{b'/2} \sqrt{1 + \left(\frac{dz}{dy}\right)^2}\, dy > b \tag{35}$$

An increase in structural weight would necessitate operation of the curved wing at a higher lift condition, and the induced drag of the wing would then increase.

Since the bending-moment magnitude and distribution of a curved wing can influence both the structural weight and the profile drag (through the effect on the minimum allowable profile thickness) of the wing, it is of interest to examine the quantitative effects introduced by curvature on the bending moments. In particular, the magnitudes of the bending moments of a cambered wing as compared with those of a flat wing are of interest.

The Bending-Moment Distribution for a Flat-Span Wing

The optimum distribution of the lift loading intensity necessary for minimum induced drag for a flat lifting line is elliptical in form, and the corresponding circulation distribution is given by

$$\Gamma(y) = \Gamma_o \left[1 - \left(\frac{y}{b'/2}\right)^2\right]^{1/2} \tag{36}$$

The nondimensional bending-moment distribution of the flat span can therefore be determined from equation (22) by using the nondimensional form of equation (36)

$$\frac{\Gamma}{\Gamma_o}(\sigma) = \left(1 - \sigma^2\right)^{1/2} \tag{37}$$

and the value 1.57 for B. In this simple case equation (22) can be directly integrated with the result

$$M'_f(\gamma) = 0.637\left[\frac{\gamma^2}{2}\sqrt{1 - \gamma^2} + \frac{\gamma}{2}\sin^{-1}\gamma + \frac{1}{3}\sqrt{\left(1 - \gamma^2\right)^3} - \frac{\pi}{4}\gamma\right] \tag{38}$$

This function is plotted in figure 10. The dimensional moment distribution $M_f(y)$ is obtained from this figure for any elliptically loaded wing by multiplying the M'_f value at a particular station $\left(y = \gamma \frac{b'}{2}\right)$ by $W \frac{b'}{2}$, the reference moment of the wing. It is of course obvious that the distribution of figure 10 is identical with the distributions for $\beta = 0$ in figures 5 and 8, since equations (28) and (33) both reduce to the distribution for a straight line when $\beta = 0$.

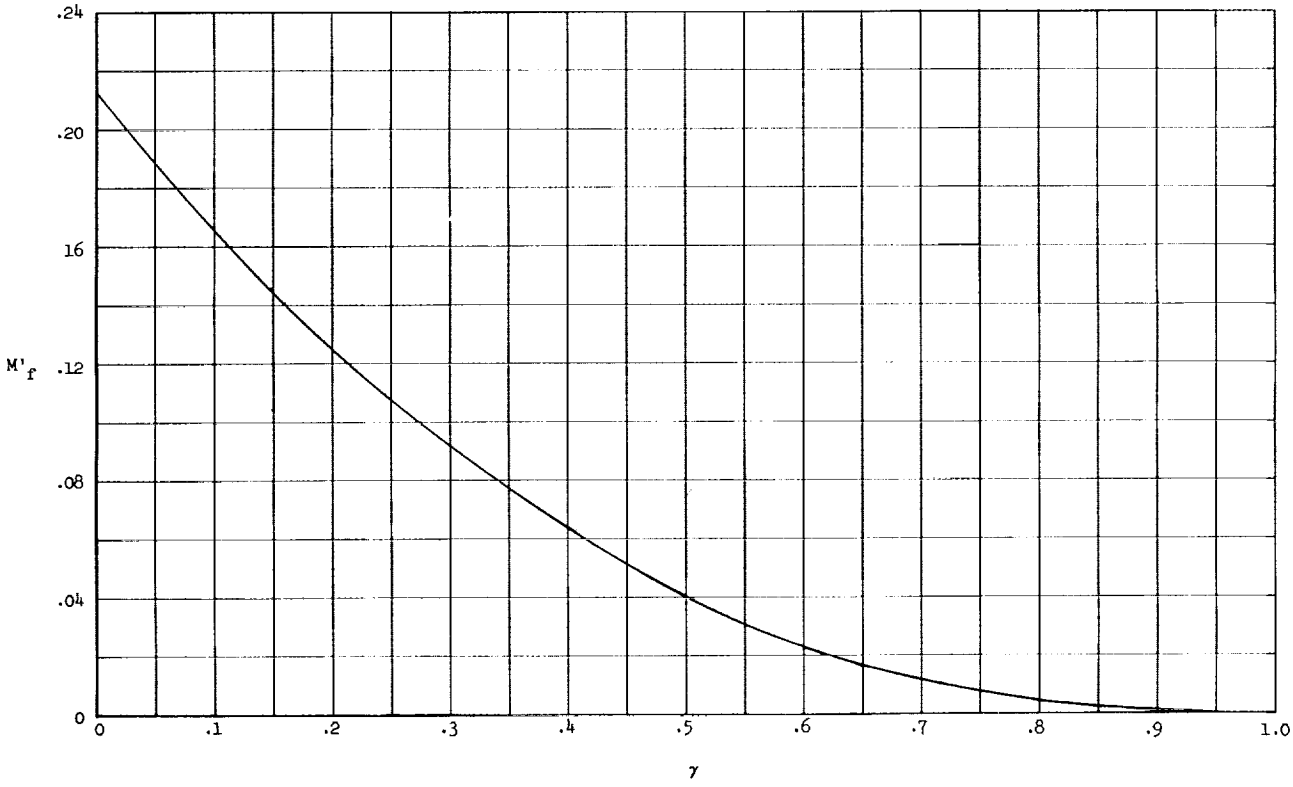

Figure 10.- Bending-moment distribution for the flat span.

Comparison of the Bending Moments of Flat and Curved Wings

For purposes of comparison, the moment distribution of any cambered wing can be divided by that of the optimally loaded flat wing of equal projected span b' and furnishing the same vertical lift force. Under such conditions,

$$\frac{M_c}{M_f} = \frac{M'_c}{M'_f}(\gamma) \tag{39}$$

where the subscripts c and f refer respectively to the cambered- and flat-span wings. A plot of the function M'_c/M'_f of equation (39) explicitly shows the effects of camber on the local bending moment. For values of the ratio greater than 1.0, of course, the moment of the cambered wing will exceed that of the flat wing, for equal total lift forces.

Plots of the bending-moment ratio for the families of circular-arc and semiellipse forms are shown in figures 11 and 12, respectively. It is seen that increased curvature causes large increases in the bending-moment ratios over the outboard portion of the spans. The root bending moment ($\gamma = 0$) also increases with increasing camber, but not as rapidly as for the outboard sections of the wing. The dashed segments of the curves in these figures are extrapolations beyond the last calculated point at $\gamma = 0.9$.

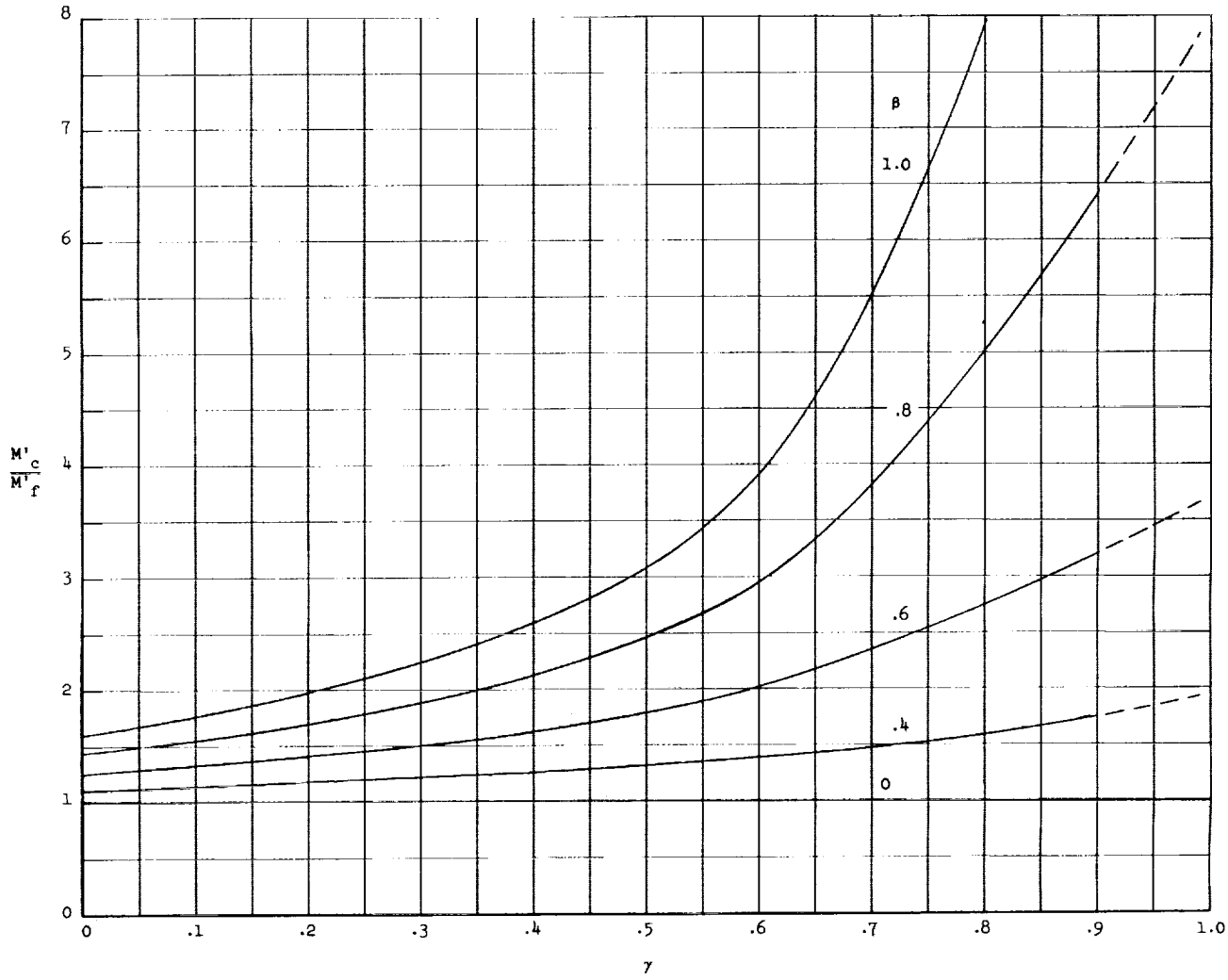

Figure 11.- Bending-moment ratio distributions for circular arcs.

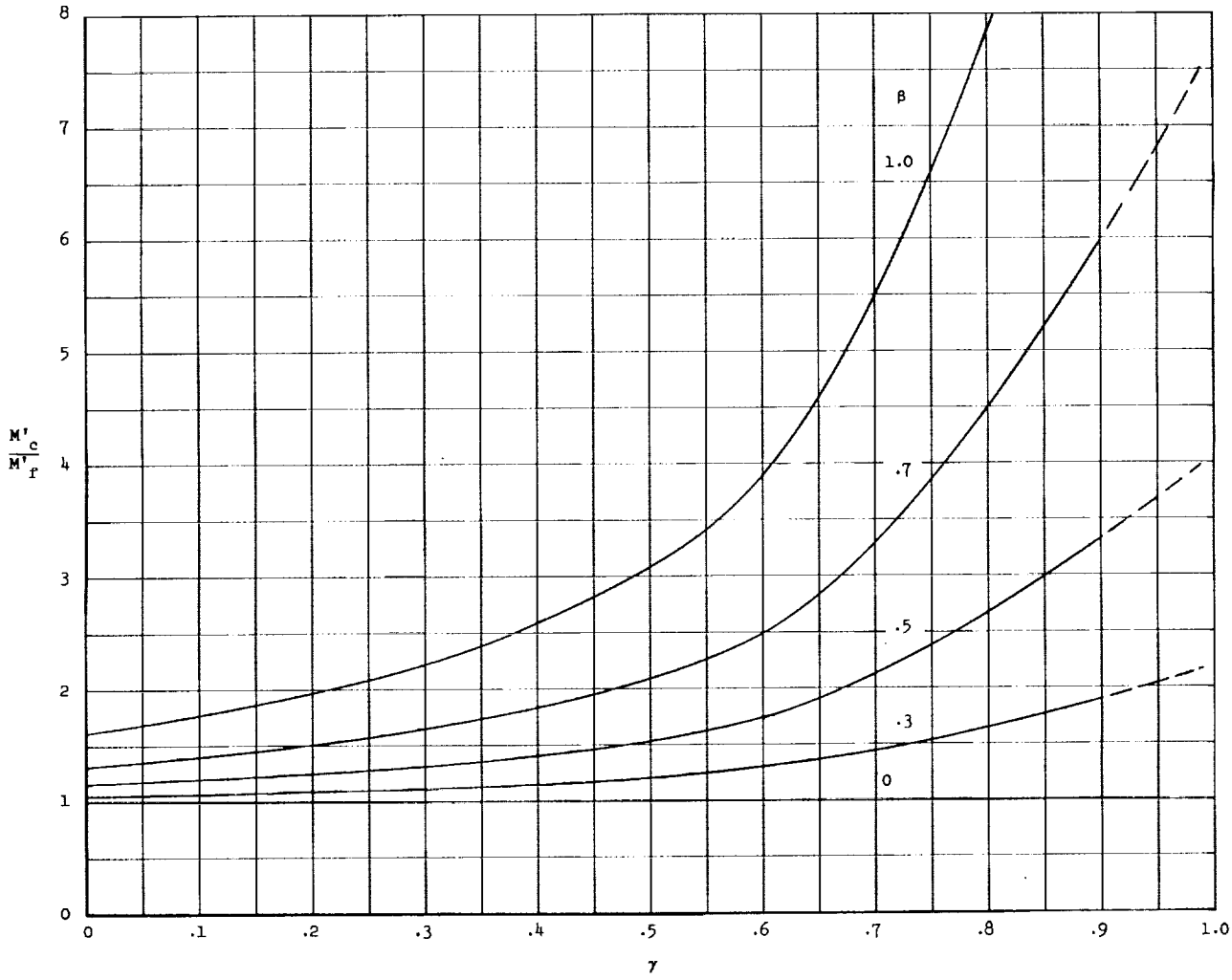

Figure 12.- Bending-moment ratio distributions for semiellipses.

The reason for the increased bending-moment ratio on the outer sections of the wings is evident from figure 13. Because of the large value of the projected vertical height of span compared with the projected horizontal length (corresponding to the flat span wing), the effective moment-producing force of the cambered wing is much larger.

Relation Between the Bending Moment and Induced-Drag Efficiency

The foregoing comparisons have been made on the basis of equal projected spans for the cambered and flat wings ($\psi = 1.0$). With this particular restriction, the cambered wing will have less induced drag for the same lift, since k is greater than 1.0 for the case b' = b. However, as shown in equation (50) of reference 1, $k = C_l/\psi^2$ (where $\psi = b/b'$) and the relative efficiency of the cambered wing depends upon the length of its projected span b' compared with

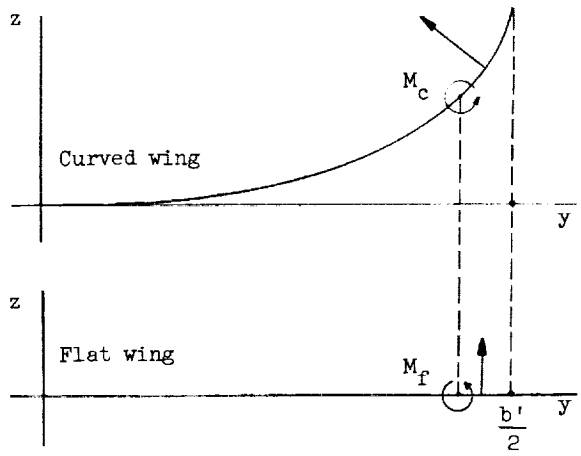

Figure 13.- Force and moment comparisons for curved and flat wings.

the span b of the flat reference wing. Since the bending-moment ratio M_c/M_f is also a function of ψ, the relative bending moment can be directly related to the wing efficiency.

The bending-moment ratio, when written for the general case where the wings have equal lift loads but different projected span lengths, is obtained as a function of ψ from the expression

$$\frac{M_c}{M_f} = \frac{b'/2}{b/2} \frac{M'_c}{M'_f}(\gamma) = \psi^{-1} \frac{M'_c}{M'_f}(\gamma) \tag{40}$$

Then, since $\psi = \sqrt{C_l/k}$ (where C_l is the value of k when the semispans of cambered and flat wings are equal, i.e., when $\psi = 1$) equation (40) can be written as a function of the cambered-wing efficiency. Thus,

$$\frac{M_c}{M_f} = \sqrt{\frac{k}{C_l}} \frac{M'_c}{M'_f}(\gamma) = \sqrt{k}P(\gamma) \tag{41}$$

In equation (41), C_l and M'_c/M'_f are functions only of the form and β value of the particular camber line, for a given value of γ. Thus, equation (41) gives the moment ratio at equal fractions of the respective semispans (i.e., equal values of γ) for all values of k. Since $P(\gamma)$ is uniquely determined for each member of any particular family of camber forms by specifying a value for β, equation (41) allows the determination of the bending-moment variation of the curved wing with its induced-drag efficiency (or projected semispan length $b'/2$). From the equation, it is obvious that the ratio of the bending moment of the curved wing at a given fraction of the semispan $b'/2$ to that of the flat wing at an equivalent spanwise station will, for equal total lift forces, increase as the efficiency k increases.

As an example of the use of equation (41), the bending-moment ratio is calculated for the root station ($\gamma = 0$) for the semiellipse camber line with $\beta = 0.5$, for $k = 1.0$. This means that the flat wing and curved wing have equal lift and induced drag forces, and that the semispan of the curved wing is $\frac{1}{\sqrt{C_l}}$ or $\frac{1}{\sqrt{1.31}}$ times that of the flat wing. Thus, with use of figure 12,

$$\frac{M_c}{M_f} = \frac{1.16}{\sqrt{1.31}} = 1.02 \tag{42}$$

and it is seen that the root bending moment of the cambered wing is 2 percent larger than that of the flat wing.

EFFECT OF BENDING MOMENT ON SECTION PROFILE THICKNESS

The bending-moment distribution of a cambered wing has an effect on the profile drag of the wing through the thickness ratio of the section profiles. The thickness distribution is dictated by the need to provide sufficient depth within the profile for housing the wing spar. It is of course possible to make the spar very thin for a given moment of inertia of its section, but then the increase in induced drag due to the increased spar weight tends to cancel any drag reduction due to the use of thin profiles. Thus, in general, there exists an optimum spar geometry which will result in minimum total wing drag. Although a complete analysis for determining the optimum spar geometry is possible, including both drag and weight effects, the following elementary considerations are restricted to an analysis of the effects of the bending moment on the profile drag only.

The Profile-Thickness Distribution

It is assumed herein that the spar of the camber-span wing is designed on the basis of supporting a specified ultimate design load W_D and that the load and bending-moment distributions correspond to optimum loading conditions. The basic design relation for the spar is then given by the allowable stress condition

$$\theta_{max} \geqq \frac{M_{max}}{Z} \tag{43}$$

where θ_{max} is the maximum allowable flexural stress in the spar material, M_{max} is the local bending moment corresponding to the ultimate load W_D, and Z is the section modulus. The section modulus is defined by

$$Z = \frac{I}{h} \tag{44}$$

where I is the area moment of inertia of the section about the neutral axis and h is the distance from the neutral axis to the outermost element of the spar section.

For common symmetrical spar sections, such as rectangles, squares, and those composed of elements of such forms, the neutral axis passes through the centroid of area only in the absence of a resultant-force component along the local axis of the spar. With cambered wings, the curvature of the span introduces an axial force along the spar, and for symmetrical sections the neutral axis will be below the centroid of area. However, in cases where the camber is moderate, the side forces produced by the curvature are relatively small and the distance h in equation (44) can be assumed equal to $\frac{1}{2}t$, where t is the total spar depth. For a specified section geometry, the area moment of inertia is

$$I = C_2 t^4 \tag{45}$$

where C_2 is a constant characteristic of the geometry. From equation (44) the section modulus becomes

$$Z = \frac{C_2 t^4}{t/2} = \epsilon t^3 \tag{46}$$

Substituting equation (46) into equation (43) gives the maximum-stress relation as

$$\epsilon t^3 \geqq \frac{M_{max}}{\theta_{max}} = \omega \tag{47}$$

This equation indicates the primary effects of the bending-moment distribution. If t is made large, ϵ can be made very small and a light spar weight can be obtained. However, a large value of t may cause an increase in profile drag. On the other hand, a small value of t, while reducing the profile drag, will require a large value for ϵ with an accompanying increase in spar weight. When a particular value of ϵ is specified, the minimum allowable value of t is determined as

$$t \geqq \sqrt[3]{\omega/\epsilon} \tag{48}$$

From equations (47) and (48) it is seen that the thickness t varies with the cube root of the bending moment. Hence, it follows from equation (39) that the relative minimum profile thicknesses of cambered and flat wings will be proportional to the cube root of their moments, and that even though the moment ratio may be large, the thickness ratio of the two wings can still be relatively small. From a practical application standpoint, the increased thickness required for the spars of cambered wings may not prove especially detrimental since a number of profiles having very low drag at high thickness ratios exist. (See ref. 2.)

The Minimum Profile Drag

With a particular thickness distribution determined on the basis of equation (48), the effects of $t(y)$ on the profile drag of the wing can be determined, and the optimum chord distribution $c_{opt}(y)$, or $c_{opt}(s)$, can be established for minimum profile drag at cruise flight conditions. As shown in reference 2, a cambered-span wing will possess minimum induced drag when the span loading intensity $F'(s)$ is such that equation (2) of the present paper applies. The condition which must be satisfied for minimum induced drag at cruise is therefore

$$F' = c_l q c \tag{49}$$

where F' is determined by the cruise weight W and q is determined by the flight speed and altitude. The corresponding profile-drag intensity D_o' is given by

$$D_o' = c_d q c \tag{50}$$

where c_d is obtained from the section drag polar $c_d(c_l)$.

In order to establish the optimum chord length for minimum profile drag, a range of chord values is determined by substitution of various values for μ in the thickness-ratio function

$$\frac{t}{c} = \mu \tag{51}$$

where t is now assumed to be a known function of y (or s) for the wing. Then, by using equation (49) in the form

$$\frac{F'}{q} = c_l c \tag{52}$$

a value of c_l can be determined for each value of c. From the section polar for each particular value of $t/c = \mu$ for the family of profiles under consideration, the value of c_d corresponding to the c_l value can be read. Substitution of the corresponding values of c_d and c into equation (50) allows the calculation of the section profile drag D_o'. A plot of D_o' as a function of c (such as sketched in fig. 14) then reveals the optimum value of the chord c_{opt} for minimum D_o' for the family of profiles specified by the range of values of μ.

By use of the foregoing procedure, various families of wing section profiles can be examined and the section possessing minimum profile drag at cruise for the particular thickness function $t(y)$ of the cambered wing can be determined. This procedure gives an optimum chord distribution for the conditions of cruise flight. As noted in reference 2, however, the slow-flight conditions of the

take-off and landing phases of flight may require some compromise on the area and chord distribution of the wing.

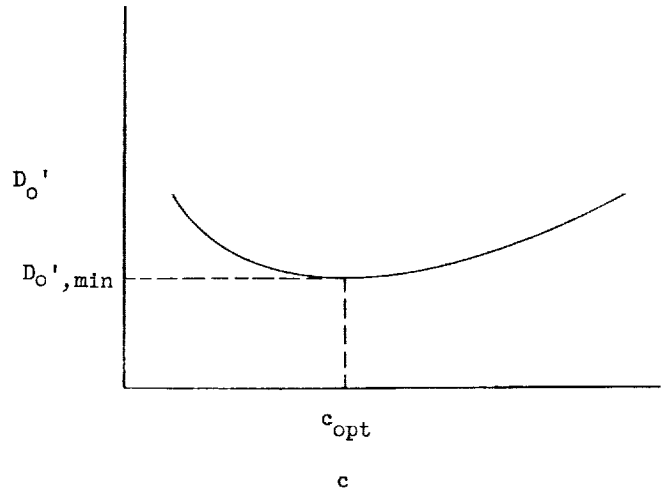

Figure 14.- Plot for determining the optimum chord length.

AEROELASTIC EFFECTS

The basic relation governing the bending deflection of a wing under aerodynamic loading is given by

$$M = \frac{EI}{R} \tag{53}$$

In equation (53) R is the radius of curvature of the spar's neutral axis in the stressed condition; the unstressed condition of the spar corresponds to a linear neutral axis, that is, $R = \infty$. In usual practice, when the wing is designed to support an ultimate load W_D (which includes a suitable factor of safety) the resulting moment-of-inertia distribution is sufficiently large that, for the bending moments normally encountered in flight, R is very large and the wing behaves essentially as a rigid structure. When cambered-span wings are designed on the basis of such procedures, it is possible that in some cases relatively thick sections can result because of the increased bending moments near the wing tip, as compared with those of flat-span wings. Since it is desirable that the profile drag of cambered wings be minimized, it may be of interest to briefly investigate the possibility of reducing the wing thickness near the tip by making the wing relatively elastic in this region.

In making the wing elastic, two basic requirements must be met. First, the thickness of the wing must be sufficiently small that the allowable stress is not exceeded. Thus, when the tensile stress in the spar is considered as the limiting factor,

$$t \leqq \frac{2}{n} \frac{R}{E} \theta_{max} \tag{54}$$

where n is a factor which specifies the neutral-axis location of the section. (Because of the axial load on the spar of a cambered wing, the neutral axis will not pass through the geometrical center of the section.) The second requirement is that the section moment of inertia be such as to allow the desired curvature, that is,

$$I = \frac{RM}{E} \tag{55}$$

If the value of R is reduced, the required value of I can be correspondingly reduced and, hence, the thickness can be lowered. In this equation I is the moment of inertia of the section about the neutral axis and, for a given section geometry, it will generally have a larger value for a cambered wing (because of the factor n) than for a flat wing. (No account has been taken of the effects on spar weight in these simple considerations. In general, however, increases in the flexibility of a wing structure are accompanied by decreases in structural weight.)

If the elastic tip region of a partially flexible cambered wing is designed to attain its curvature $z(y)$ by deforming under the design cruise flight load W_c from an initially unstressed condition (where $R = \infty$), the local radius of curvature of the neutral axis will be the same as that of the desired camber-line form $z(y)$ and, therefore,

$$R = \frac{ds}{d\tau} = \left[1 + \left(\frac{dz}{dy}\right)^2\right]^{3/2} \left(\frac{d^2z}{dy^2}\right)^{-1} \tag{56}$$

For certain cambered-wing forms, R can thus assume relatively small values. For example, the radius of curvature of circular-arc segments is obtained from equation (27)

$$\frac{R}{b'/2} = \frac{1 + \beta^2}{2\beta} \tag{57}$$

Thus, $\infty \geqq \frac{R}{b'/2} \geqq 1$ when $0 \leqq \beta \leqq 1$, and the local radius of curvature is constant along the span. The local radius of curvature of a semiellipse is given in nondimensional form by

$$\frac{R}{b'/2} = \frac{\left\{1 + \left[\beta\gamma\left(1 - \gamma^2\right)^{-1/2}\right]^2\right\}^{3/2}}{\beta\left[\gamma^2\left(1 - \gamma^2\right)^{-3/2} + \left(1 - \gamma^2\right)^{-1/2}\right]} \tag{58}$$

A plot of equation (58) is presented in figure 15 for the particular case $\beta = 0.5$, and it is seen that the local radius of curvature is quite small especially near the wing tips.

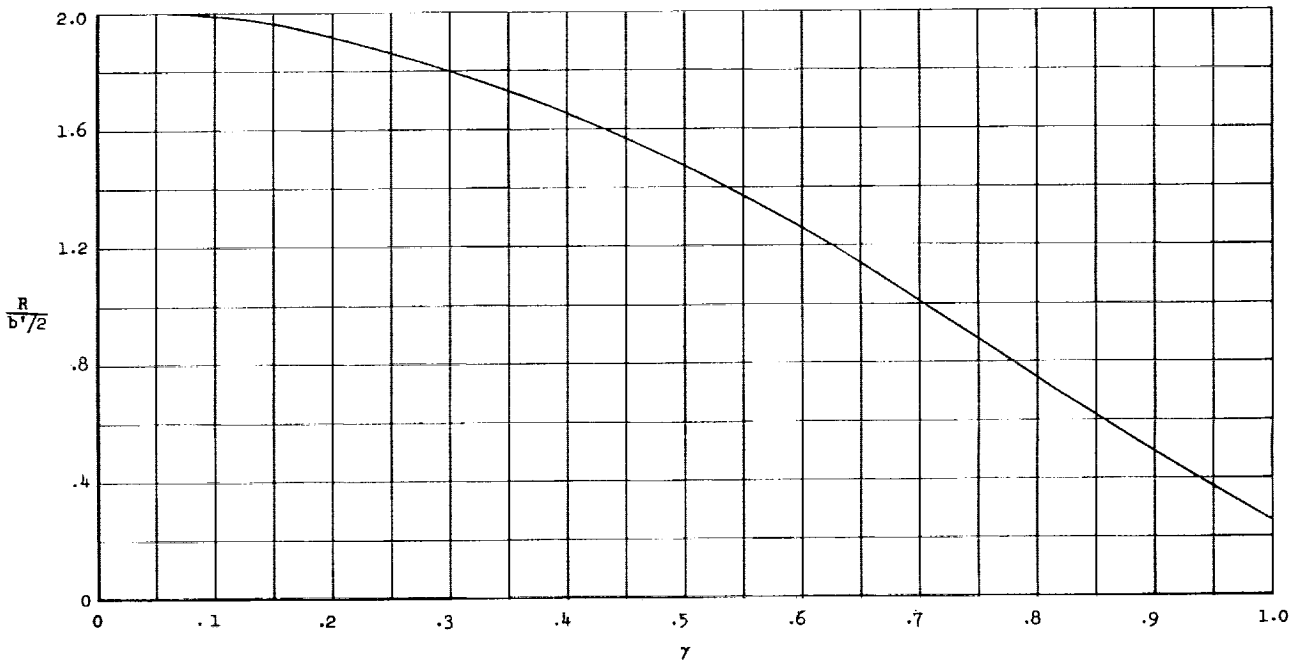

Figure 15.- Local radius of curvature of the $\beta = 0.5$ semiellipse form.

There are obviously a number of fundamental problems associated with the use of elastic wings, one of the most important being the provision for an adequate ultimate strength factor. For elastic wings designed to accommodate a flight load W_c, it would be necessary that the wing deformation under loads greater than W_c be such that $\frac{\partial M}{\partial W} \leqq 0$. This requirement could conceivably be satisfied by special aeroelastic design of the wing tip regions.

CONCLUDING REMARKS

By use of the relations developed herein, the bending-moment distributions for an optimum cambered-span wing system can be determined and the results used to establish the basic structural requirements of the wing. Subsequently, the effects of the structural characteristics on the wing profile drag can be determined, and the optimum chord distribution for cruise flight can be calculated. The resulting aerodynamic efficiency of the cambered wing can then be compared with that of the flat reference wing and the relative efficiencies evaluated.

For more detailed and exact comparisons, of course, it will be necessary to consider the effects of the structural weight on the resultant induced drag.

The simple structural analyses of this paper are based on the wing bending moment alone. In some cases, the torsional and shear loads, rather than the bending moment, may govern the spar thickness and weight. In any event, a complete analysis must necessarily involve simultaneous consideration of all loads.

The results of the calculation of the bending-moment distributions for simple circular-arc and semiellipse camber forms indicate that somewhat thicker spars may be required for cambered wings, but that for moderate curvatures this increase is not practically significant.

Langley Research Center,
National Aeronautics and Space Administration,
Langley Station, Hampton, Va., November 7, 1962.

APPENDIX

DERIVATION OF THE ARC LENGTH OF AN ELLIPSE

The parametric equations of the ellipse, in terms of the eccentric angle φ, are given by

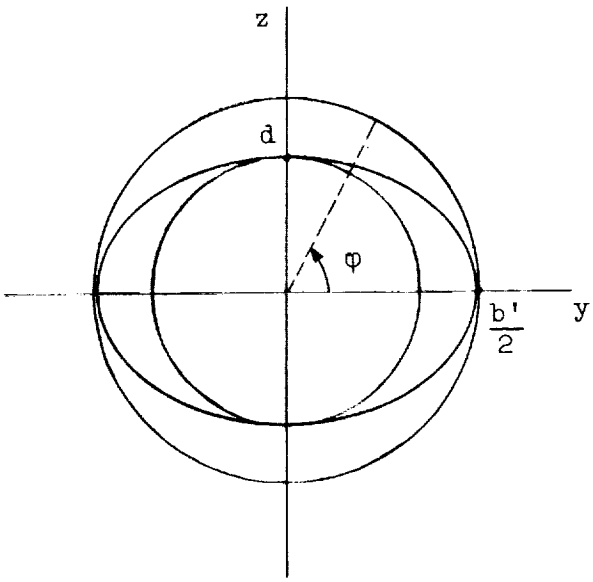

$$\left.\begin{aligned} y &= \frac{b'}{2}\cos\varphi \\ z &= d\sin\varphi \end{aligned}\right\} \tag{A1}$$

The geometrical relations used in determining the arc length of the ellipse forms are shown in the sketch. Differentiating equation (A1) gives

$$\left.\begin{aligned} \frac{dy}{d\varphi} &= -\frac{b'}{2}\sin\varphi \\ \frac{dz}{d\varphi} &= d\cos\varphi \end{aligned}\right\} \tag{A2}$$

whence

$$\frac{dz}{dy} = -\frac{d}{b'/2}\operatorname{ctn}\varphi \tag{A3}$$

Substituting equation (A3) into equation (15) yields the result

$$s = \frac{b'}{2}\int_{\varphi}^{\pi/2}\left[\sin^2\varphi + \left(\frac{d}{b'/2}\right)^2\cos^2\varphi\right]^{1/2} d\varphi \tag{A4}$$

In equation (A4) the arc length s is considered positive in the positive y-direction (i.e., in the direction of decreasing φ). Use of the definition $\beta = \frac{d}{b'/2}$ in equation (A4) yields

$$\frac{s}{b'/2} = \int_{\varphi}^{\pi/2}\left[\sin^2\varphi'\left(1 - \beta^2\right) + \beta^2\right]^{1/2} d\varphi' \tag{A5}$$

Integration of equation (A5) can be carried out numerically, by using the relation $\varphi = \cos^{-1}\frac{y}{b'/2}$ from equation (A1), to obtain the function $s(y)$ for the ellipse form. This integration has been carried out for the family of semi-ellipses $0 \leqq \beta \leqq 1$, and the results are presented in figure 9.

REFERENCES

1. Cone, Clarence D., Jr.: The Theory of Induced Lift and Minimum Induced Drag of Nonplanar Lifting Systems. NASA TR R-139, 1962.

2. Cone, Clarence D., Jr.: The Aerodynamic Design of Wings With Cambered Span Having Minimum Induced Drag. NASA TR R-152, 1963.